



HAL
open science

A monodisperse model for water bubbles growth in magmas

Alain Burgisser, Louis Forestier-Coste, François James, Simona Mancini

► **To cite this version:**

Alain Burgisser, Louis Forestier-Coste, François James, Simona Mancini. A monodisperse model for water bubbles growth in magmas. 2010. hal-00544506v1

HAL Id: hal-00544506

<https://hal.science/hal-00544506v1>

Preprint submitted on 8 Dec 2010 (v1), last revised 13 Jan 2012 (v3)

HAL is a multi-disciplinary open access archive for the deposit and dissemination of scientific research documents, whether they are published or not. The documents may come from teaching and research institutions in France or abroad, or from public or private research centers.

L'archive ouverte pluridisciplinaire **HAL**, est destinée au dépôt et à la diffusion de documents scientifiques de niveau recherche, publiés ou non, émanant des établissements d'enseignement et de recherche français ou étrangers, des laboratoires publics ou privés.

A monodisperse model for water bubbles growth in magmas

A. Burgisser^{*}, L. Forestier-Coste[†], F. James[†], S. Mancini^{*,†}

Abstract

Growth of gas bubbles in magmas may be modelled by a system of differential equations coupled with an advection-diffusion equation, see [10], and characterised by two relaxation times linked to the viscosity of the magma and to the diffusivity of the dissolved gas, respectively. Here, we propose a numerical scheme which, unlike previously published schemes, preserves the total mass of the coupled system of equations. We also study the asymptotic behavior of the system of equations, when letting the relaxation times vary from 0 to ∞ , and show the numerical convergence of the solutions obtained by means of the general numerical scheme to the simplified asymptotic limits. Finally, we validate and compare our numerical results with those obtained in experiments.

1 Introduction

All volcanic eruptions involve a decompression of the magma during its ascent from the Earth's crust to the surface. This decompression causes the volatiles dissolved into the magma to come out of solution as gas bubbles. The way these bubbles are growing, whether they coalesce with one another or travel faster than or with the magma, are all conditioning the way the volcanic eruption will unfold. Bubbles that remain trapped with the magma they originally grew from will accumulate gas pressure until failure of the magma releases it suddenly to produce an explosive eruption. Such scenario

^{*}ISTO-OSUC (Institut des Sciences de la Terre d'Orléans - Observatoire des Sciences de l'Universe region Centre), UMR 6113, University of Orléans and CNRS, F-45067 Orléans, France

[†]Fédération Denis Poisson (FR 2964), MAPMO (UMR 6628), BP. 6759, University of Orléans and CNRS, F-45067 Orléans, France

is most likely when the magma is highly viscous and prevails bubble motion. This situation is propitious to modelling because bubble can be considered as immobile in the magma and the resulting spherical geometry allows one to reduce bubble growth to a 1D system of differential equations describing the evolution of pressure and gas mass in a bubble coupled with an advection-diffusion equation describing the drainage of the dissolved gas towards the bubble. A further assumption is that bubbles are exclusively made of water vapour, which can be justified by the fact that water is, by far, the most abundant volatile species in such viscous magmas.

Since the seminal work done in [14], several numerical scheme that solve such system of differential equations have been proposed (see [1, 16, 17, 3, 13]). Application to gas bubble in magmas is slightly more recent (see [12, 11, 15, 4, 10, 5]). All these schemes have in common a discretization of the advection-diffusion equation that is not strictly conservative with respect to the diffused species. They also involve user-defined discretization parameters that have to be empirically adjusted to ensure sufficient convergence and/or accuracy of the scheme. Developing alternate, robust schemes would allow including the dynamics of bubble growth into more sophisticated model that take into account, for instance, that bubble have different sizes, or that, if magma viscosity is low enough, bubble may rise with respect to the magma.

The present work is developed as follows. In section 2, we recall the differential equations describing the respective evolution of bubble radius and mass, together with the advection-diffusion equation concerning the behavior of the water concentration in the magma. Following [10], we write the problem in dimensionless form, introducing the relaxation times Θ_V and Θ_D . Section 3, is devoted to the numerical approximation of the model. The main novelty is the discretization of the advection-diffusion equation, see 3.2, in which we explain how to compute the mesh and flux at each iteration. In section 4 we deal with the asymptotic of the dimensionless problem, when the rate between the relaxation times tends to 0 or ∞ . Three main regimes are underlined: viscous, diffusive, and equilibrium. For each limit, we also give the way we shall discretize it. The numerical results, the convergence of the solution towards the simplified asymptotic limits, and the comparison with experiments are discussed in section 5. Finally, in section 6, we summarise our study and suggest possible extensions of the modelling of bubbles growth in magma.

2 The model

We are interested in the modelling of bubbles growth in magma, which are mainly composed of water vapour. Two main physical processes are at the origin of their growth. Magma is moving towards the surface and therefore it undergoes decompression. This causes, on one hand, expansion of the gas trapped into the bubble, and, on the other hand, diffusion of the water dissolved in the magma into the bubbles. Our study is based on a recent work (see [10]), in which the authors consider spherical bubbles and describe each bubble in terms of its radius R and pressure P , proposing a model for the growth of a monodisperse set of bubbles, i.e. the radius and pressure of all the bubbles contained in a small parcel of magma evolve in the same way. In their paper, Lensky et al., also propose a dimensionless formulation of the equations, yielding to the introduction of two relaxation times Θ_V and Θ_D . We recall in the following sections the physical model and its dimensionless version.

2.1 Physics modelling

Let assume that bubbles are spherical, with a radius $\hat{R} = \hat{R}(t)$ and a pressure $\hat{P} = \hat{P}(t)$. Let us consider that each bubble is surrounded by a bigger sphere of radius $\hat{S} = \hat{S}(t)$, which we call the influence region. This region represents the volume of magma interacting with the bubble, i.e. the water contained in the magma in this region will diffuse into the bubble. It is thus natural to consider water mass conservation in the water exchange bubble-magma: the total mass, \mathcal{M} , given by the sum of the water mass in a bubble and of the water contained in its influence region must be equal to the water mass at initial time, for example when no bubbles are present in the magma. This may be expressed in the following form:

$$\frac{4\pi\hat{\rho}}{3}\hat{R}^3 + 4\pi\hat{\rho}_m \int_{\hat{R}(\hat{t})}^{\hat{S}(\hat{t})} \hat{r}^2 C d\hat{r} = \frac{4\pi\hat{\rho}_m}{3}\hat{S}_0^3 C_0. \quad (1)$$

In (1) $\hat{\rho}$ and $\hat{\rho}_m$ are respectively the density of the gas and the magma, the function $C = C(\hat{r}, \hat{t})$ represents the concentration of water in the magma, and depends on time \hat{t} and on the space/radial variable $\hat{r} \in [\hat{R}(\hat{t}), \hat{S}(\hat{t})]$, i.e. the radial distance from the boundary of the bubble, \hat{S}_0 is the radius of the influence region assuming that the bubble has zero radius \hat{R} , and C_0 is the concentration of water assuming that the radius \hat{R} is zero.

Remark 2.1 *With the above definition for the influence region, the magma porosity, here denoted by $\alpha = \alpha(\hat{t})$, is given by:*

$$\alpha = \frac{\hat{R}(\hat{t})^3}{\hat{S}(\hat{t})^3}.$$

□

Following [10], we describe the set of equations governing bubble growth. We begin by describing the equations governing the evolution of the bubble radius \hat{R} and pressure \hat{P} ; after we consider the evolution of the water concentration C in the influence region; finally we describe the assumptions on the behavior of the influence region radius \hat{S} and on the ambient pressure (the magma pressure) $\hat{P}_a = \hat{P}_a(t)$. We refer the reader to table 1 for a description of the physical parameters of this modelling.

We assume that the bubbles are non-interacting and mono-disperse, therefore the evolution of a single bubble describes that of the set of bubbles. From the conservation of the first moment of Navier-Stokes equations, we have that the variation of the pressure, the surface tension and the viscosity terms must satisfy the following:

$$\hat{P} = \hat{P}_a + \frac{2\sigma}{\hat{R}} + 4\frac{\dot{\hat{R}}}{\hat{R}}\hat{\eta}, \quad (2)$$

where \hat{P}_a is the ambient pressure, σ is the surface tension and $\hat{\eta}$ is the magma viscosity, which will be assumed constant in this paper.

We note that, inside the bubble, water is in gaseous form and may be considered as a perfect gas, hence from the perfect gas law:

$$GT\hat{\rho} = \hat{P}M_m, \quad (3)$$

with M_m the molar mass for water, G the perfect gas constant and T the gas temperature.

The pressure inside a bubble depends on the bubble radius, as shown by (2), but also on the water mass inside the bubble. Mass may vary because of the diffusion of water from the surrounding magma into the bubble. Hence, we have the following balance equation:

$$\frac{4\pi}{3} \frac{d}{d\hat{t}} \left(\hat{\rho} \hat{R}^3 \right) = 4\pi \hat{\rho}_m (F)_{\hat{r}=\hat{R}}, \quad (4)$$

where F represents the water flux from the magma into the bubble and it will be described later on, see (7).

We now model what happens in the influence region by giving the equation governing the evolution of the water concentration in this region. This leads also to an explicit formulation for the flux F . Water in the magma diffuses; hence, in the influence region, we can model the concentration of water $C = C(\hat{r}, \hat{t})$, depending on time \hat{t} and on the distance $\hat{r} \in [\hat{R}(\hat{t}), \hat{S}(\hat{t})]$, by means of the following advection-diffusion equation expressed in radial co-ordinate:

$$\frac{dC}{d\hat{t}} = \frac{1}{\hat{r}^2} \frac{\partial}{\partial \hat{r}} \left(\hat{r}^2 \hat{D} \frac{\partial C}{\partial \hat{r}} \right), \quad (5)$$

where \hat{D} is the magma diffusion coefficient, assumed constant in this work, and $dC/d\hat{t}$, is the total derivative, representing the time variation and the advection term. Taking into account the displacement of the bubble border with radial velocity $\dot{\hat{R}}\hat{R}^2/\hat{r}^2$, the total time derivative $dC/d\hat{t}$ in (5) is given by:

$$\frac{dC}{d\hat{t}} = \frac{\partial C}{\partial \hat{t}} + \dot{\hat{R}} \frac{\hat{R}^2}{\hat{r}^2} \frac{\partial C}{\partial \hat{r}}. \quad (6)$$

It follows that the flux $F = F(\hat{r}, \hat{t})$ in equation (4) is given by:

$$F = \hat{r}^2 \hat{D} \frac{\partial C}{\partial \hat{r}} \quad (7)$$

To complete the modelling of the behavior of the water concentration C in the influence region, we consider the following boundary conditions:

$$C(\hat{R}, \hat{t}) = K_H \sqrt{\hat{P}}, \quad (8)$$

determining the water concentration on the bubble border, $\hat{r} = \hat{R}$, in terms of the solubility equation, and where we denote by K_H the Henry constant;

$$\left. \frac{\partial C}{\partial \hat{r}} \right|_{\hat{r}=\hat{S}} = 0, \quad (9)$$

asserting that the flux of water concentration on the outer border, $\hat{r} = \hat{S}$, of the influence region is null.

Finally, we have to describe the behavior of the ambient pressure \hat{P}_a and of the influence region radius \hat{S} . Since one of the goals of the present study is to compare our numerical results with those obtained in experiments, we

assume that, after the bubbles nucleation, pressure is linearly decreased from an initial value P_i and with a constant decompression rate ΔP . Hence the ambient pressure \hat{P}_a is governed by the following equation:

$$\hat{P}_a(\hat{t}) = P_i - \hat{t}\Delta P. \quad (10)$$

Concerning the time evolution of the radius of the influence region \hat{S} , and from the assumption that the volume of the influence region is constant in time (see [10]), we have:

$$\hat{S}(\hat{t}) = \left(\hat{S}_0^3 + \hat{R}(\hat{t})^3 \right)^{1/3}, \quad (11)$$

where \hat{S}_0 is a constant representing the initial radius of the influence region, for example when the bubble has a null radius \hat{R} .

We resume, in table 1, the meanings, physical values and order of magnitude of the constants and parameters considered in our model and computations.

Table 1: Constants

D	Diffusivity	$10^{-12} (m^2 \cdot s^{-1})$
η	Viscosity	$10^4 (Pa \cdot s)$
M	Molar Mass for Water	$18.10^{-3} (kg \cdot mol^{-1})$
G	Perfect Gas Constant	$8.3144 (J \cdot mol^{-1} \cdot K^{-1})$
T	Temperature	$1098.15 (K)$
σ	Surface Tension	$0.1 (J \cdot m^{-2})$
ρ_m	Magma density	$2154 (kg \cdot m^{-3})$
K_H	Henry Constant	$3.44 \cdot 10^{-6} (kg^{-1/2} \cdot m^{1/2})$
S_0	Influence Radius for $R = 0$	$6.204 \cdot 10^{-5} (m)$
ΔP	Decompression Rate	$10^5 (Pa \cdot s^{-1})$
P_i	Initial Ambient Pressure	$10^8 (Pa)$
C_0	Water Concentration for $R = 0$	$4.21 (wt.\%)$

2.2 Dimensionless problem

This section is dedicated to the dimensionless model. As we will see, we will be led to define a viscous and a diffusion relaxation time, respectively Θ_V and Θ_D , which may physically vary for several order of magnitude. Their influence on the behavior of the solutions will be discussed later on, see section 4.

As done in [10], we consider the following reference values: the initial bubble radius, R_i , the initial gas density ρ_i , the initial ambient pressure $P_i = P_a(t = 0)$ and the diffusion and viscosity coefficients, D_i and η_i . We then perform the following change of variables and parameters:

$$\begin{aligned} \eta &= \frac{\hat{\eta}}{\eta_i} & D &= \frac{\hat{D}}{D_i} & \rho_m &= \frac{\hat{\rho}_m}{\rho_i} & \Sigma &= \frac{2\sigma}{R_i P_i} \\ R &= \frac{\hat{R}}{R_i} & S &= \frac{\hat{S}}{R_i} & r &= \frac{\hat{r}}{R_i} & \dot{R} &= \frac{\hat{R} P_i}{R_i \Delta P} \\ P &= \frac{\hat{P}}{P_i} & P_a &= \frac{\hat{P}_a}{P_i} & \rho &= \frac{\hat{\rho}}{\rho_i} & t &= \hat{t} \frac{\Delta P}{P_i} \end{aligned}$$

where the new dimensionless variables and constants are denoted without the superscript. We note that, since the diffusion and viscosity coefficients are considered to be constant, we have that $D = 1$ and $\eta = 1$. Moreover, from the above definitions we obtain the following viscosity and diffusion relaxation times:

$$\Theta_V = \frac{4\eta_i \Delta P}{P_i^2}, \quad \Theta_D = \frac{R_i^2 \Delta P}{D_i P_i}. \quad (12)$$

Performing the change of variables, we end up with the following dimensionless total water mass conservation:

$$M + 3\rho_m \int_{R(t)}^{S(t)} r^2 C dr = S_0^3 C_0 \rho_m \quad (13)$$

and the dimensionless system of differential equations in R and M :

$$\dot{R} = \frac{R}{\Theta_V} \left(P - P_a - \frac{\Sigma}{R} \right) \quad (14)$$

$$\dot{M} = \frac{3\rho_m}{\Theta_D} \left(r^2 \frac{\partial C}{\partial r} \right)_{r=R} \quad (15)$$

where, we have denoted by \dot{X} the time derivative of the variable X . Moreover, the water concentration $C = C(r, t)$ must satisfy the following dimensionless advection-diffusion equation:

$$\partial_t C + \frac{\dot{R} R^2}{r^2} \partial_r C = \frac{1}{\Theta_D} \frac{1}{r^2} \partial_r (r^2 \partial_r C) \quad (16)$$

with the Dirichlet boundary condition on the bubble border:

$$C(R, t) = C_i \sqrt{\hat{P}} \quad (17)$$

where C_i is given by:

$$C_i = K_H \sqrt{P_i},$$

and the Neumann boundary condition:

$$\left. \frac{\partial C}{\partial r} \right|_{r=S} = 0 \quad (18)$$

on the outer border of the influence region.

Finally, equations (10) and (11) become, respectively:

$$P_a = 1 - t \quad (19)$$

and

$$S^3(t) = S_0^3 + R^3(t). \quad (20)$$

Remark 2.2 We note that (14) and (15) are coupled by means of the dimensionless definition of the bubble mass: $M = PR^3$, deduced from the perfect gas law. We also note that equation (15) is the differential form of the total water mass conservation (13). In fact, deriving with respect to time equation (13), and taking into account (20), we get:

$$\begin{aligned} \dot{M} &= -\frac{d}{dt} \left(3\rho_m \int_{R(t)}^{S(t)} r^2 C \, dr \right) \\ &= -3\rho_m \left(\int_{R(t)}^{S(t)} r^2 \partial_t C \, dr + S^2 \frac{dS}{dt} C(S, t) - R^2 \frac{dR}{dt} C(R, t) \right) \\ &= -3\rho_m \int_{R(t)}^{S(t)} \left(r^2 \partial_t C + \frac{dR^3}{dt} \partial_r C \right) \, dr. \end{aligned}$$

Considering now (16) and (18), we end up with:

$$\dot{M} = \frac{-3\rho_m}{\Theta_D} \int_{R(t)}^{S(t)} \partial_r (r^2 \partial_r C) \, dr = \frac{3\rho_m}{\Theta_D} (r^2 \partial_r C)_{r=R},$$

which is precisely equation (15). In other words, the system of equations we are considering is mass preserving. \square

We end this section by summarising the equations we shall discretize. We will consider the coupling of the following system of differential equations on R and P :

$$\begin{cases} \dot{R} = \frac{R}{\Theta_V} \left(P - P_a - \frac{\Sigma}{R} \right) \\ \dot{M} = \frac{3\rho_m}{\Theta_D} (r^2 \partial_r C)_{r=R} \end{cases} \quad (21)$$

with the advection-diffusion equation for the water concentration C :

$$\partial_t C + \frac{\dot{R}R^2}{r^2} \partial_r C = \frac{1}{\Theta_D} \frac{1}{r^2} \partial_r (r^2 \partial_r C), \quad (22)$$

endowed by the boundary conditions (17) and (18) and the external assumption on P_a and S given by (19) and (20), respectively.

3 Numerical approximation

In this section we consider the numerical approximation of the model (21)-(22), on $R(t)$ and $M(t)$ and $C(r, t)$, together with the boundary conditions (17)-(18) and the external assumption (19)-(20). In particular, we propose a numerical scheme for the advection-diffusion equation conserving the water mass. This is a delicate point of the discretisation; the flux at the bubble border has to be carefully computed because the magnitude of the relaxation times Θ_V and Θ_D may differ of several orders. We shall first present the straightforward discretization of the system of differential equations (21) and follow by presenting the more critical problem of the advection-diffusion equation, (22), discretization.

3.1 The differential system

We describe here the basic elements of the numerical scheme for the differential system (21).

Let us first define, for $n \in \mathbb{N}$, the time t^{n+1} and the ambient pressure $P_a^{n+1} = P_a(t^{n+1})$, at the iteration step $n + 1$, respectively by:

$$\begin{aligned} t^{n+1} &= t^n + \Delta t^n, \\ P_a^{n+1} &= 1 - t^{n+1}, \end{aligned}$$

where the time step Δt^n is computed at each iteration and must satisfy some stability conditions which will be specified later on, see section 3.3. The numerical results, see section 5, will be plotted in term of the ambient pressure P_a ,

which may be considered as a time variable.

We choose a semi-implicit scheme for the discretisation of (14), i.e. the discrete bubble radius $R^n = R(t^n)$ is implicitly treated, whereas the discrete bubble and ambient pressures, $P^n = P(t^n)$ and $P_a^n = P_a(t^n)$, are treated explicitly:

$$R^{n+1} = \left(R^n - \Delta t^n \frac{\Sigma}{\Theta_V} \right) \left(1 - \Delta t^n \frac{(P^n - P_a^n)}{\Theta_V} \right)^{-1} \quad (23)$$

We discretize the equation for the mass balance at the magma-bubble interface, (15), by a semi-explicit scheme. Defining the discrete bubble mass by $M^n = M(t^n)$, and the discrete flux in $r = R$ by $F_0^n = F(R, t^n)$, we consider:

$$M^{n+1} = M^n + 3\rho_m \frac{\Delta t^n}{\Theta_D} F_0^{n+1}, \quad (24)$$

where F_0^{n+1} given by (34). We note that this formulation allows us to compute the bubble pressure by the means of:

$$P^{n+1} = \frac{M^{n+1}}{(R^{n+1})^3},$$

which is physically relevant.

Finally, we define the discrete radius of the influence region, $S^n = S(t^n)$, and the discrete porosity, $\alpha^n = \alpha(t^n)$, respectively by:

$$S^n = ((R^n)^3 + S_0^3)^{1/3}, \quad \alpha^n = \left(\frac{R^n}{S^n} \right)^3.$$

3.2 The advection-diffusion discretization

We discretize the advection-diffusion equation for the water concentration $C(t, r)$ splitting it into the transport and the diffusion steps. First from the advection equation, at each time iteration t^{n+1} we compute the advected mesh and a prediction of the concentration $C_i^{n+1/2}$ on the new mesh. Next, we use this new value to solve the diffusion part defining the flux F_0^{n+1} in such a way that the total mass \mathcal{M} is conserved.

3.2.1 Advection step

The advection step consists in the discretization of the following transport equation:

$$r^2 \partial_t C + \dot{R} R^2 \partial_r C = 0. \quad (25)$$

The goal here is to build a variable space mesh in such a way that the concentration function $C(t^n, r_i^n)$ is conserved during the advection, without excessive refinement, and to build a conservative scheme. Previous attempts, see for example the one in [11], considered a non-conservative scheme with respect to the advection-diffusion equation, in which discretization parameters have to be adjusted to ensure its convergence and accuracy. This fact yields to a large number of discretization points, in contrast with the present scheme, where, as shown in section 5, the number of discretization points can be small and the scheme is conservative by construction.

Let us consider the continuous in time problem and define the mesh points $r_i = r_i(t)$, for $i = 0 \dots N$, as follows: take any sequence K_0, \dots, K_N , with $K_0 = 0$ and $K_N = S^3$, and define:

$$r_i = ((R(t))^3 + K_i)^{1/3}. \quad (26)$$

Note that the $K_i - s$ are independent on time and that the choice of K_0 and K_N gives $r_0(t) = R(t)$ and $r_N(t) = S(t)$. In particular, the choice $K_i = \frac{i}{N} S_0^3$ satisfies both requirements, but what follows holds for any choice of K_i .

Lemma 3.1 *For $i = 0 \dots N - 1$ define the mesh r_i by (26), then the water mass concentration $C_i(t)$, on the cell $[r_i, r_{i+1}]$, is conserved at all time.*

Proof: First we note that the characteristic curves associated to the transport equation (25) are given by, for all $i = 0 \dots N$:

$$\dot{r}_i^2 \frac{dr_i}{dt} = RR^2. \quad (27)$$

Then, considering the time derivative of the integral over one discretization cell of $r^2 C(r, t)$ we have that, for $i = 0 \dots N - 1$:

$$\frac{d}{dt} \int_{r_i}^{r_{i+1}} r^2 C dr = \int_{r_i}^{r_{i+1}} r^2 \frac{\partial C}{\partial t} dr + r_{i+1}^2 \frac{dr_{i+1}}{dt} C(r_{i+1}, t) - r_i^2 \frac{dr_i}{dt} C(r_i, t).$$

This proves that choosing r_i in such a way that (27) holds, the water mass is conserved:

$$\frac{d}{dt} \int_{r_i}^{r_{i+1}} r^2 C dr = 0. \quad (28)$$

Finally, we remark that (27) is equivalent to:

$$\frac{dR^3}{dt} = \frac{dr_i^3}{dt} = \frac{dr_{i+1}^3}{dt},$$

integrating it with respect to time gives (26), which ends the proof. \square

We proceed now to the complete discretization of (25). We first give a recursive computation of the mesh points r_i^n which will be used from now on. Writing (26) at times n and $n + 1$, for $i = 0, \dots, N - 1$, we first get:

$$(r_i^n)^3 = (R^n)^3 + K_i, \quad (r_i^{n+1})^3 = (R^{n+1})^3 + K_i,$$

and then by subtraction we obtain the desired formula:

$$r_i^{n+1} = \left((R^{n+1})^3 - (R^n)^3 + (r_i^n)^3 \right)^{1/3}. \quad (29)$$

We remark that (29) is independent of the initial distribution of points r_i^0 , and so any choice of distribution points r_i^0 is convenient. In the computations we will present later on, we have chosen a uniform distribution for the r_i^0 . Finally, we denote by Δr_i^n the (non uniform) space discretization step, $\Delta r_i^n = r_{i+1}^n - r_i^n$.

We assume that $C(r, t) = C_i^n$ for $(t, r) \in [t^n, t^{n+1}[\times]r_i, r_{i+1}[$, and we define the prediction $C_i^{n+1/2}$ on the advected mesh at t^{n+1} from the discrete version of (28), which writes

$$\int_{r_i^n}^{r_{i+1}^n} r^2 C(t^n, r) dr = \int_{r_i^{n+1}}^{r_{i+1}^{n+1}} r^2 C(t^{n+1}, r) dr.$$

Since in each mesh $]r_i^n, r_{i+1}^n[$, $C(t^n, r) = C_i^n$, the above integrals are explicitly computed, yielding to:

$$\frac{(r_{i+1}^n)^3 - (r_i^n)^3}{3} C_i^n = \frac{(r_{i+1}^{n+1})^3 - (r_i^{n+1})^3}{3} C_i^{n+1/2}$$

Moreover, from the definition of the mesh discretization, it follows that $(r_{i+1}^n)^3 - (r_i^n)^3$ is independent with respect to time (but not with respect to the position), so that the prediction $C_i^{n+1/2}$ is defined by:

$$C_i^{n+1/2} = C_i^n. \quad (30)$$

3.2.2 Diffusion step

We now discretize the diffusion equation:

$$r^2 d_t C = \frac{1}{\Theta_D} \partial_r (r^2 \partial_r C).$$

Integrating the above equation on the interval $[t^n, t^{n+1}[\times]r_i, r_{i+1}[$, considering that $d_t C$ is constant on each mesh, and recalling (30), we obtain, for $i = 1 \dots N - 1$:

$$C_i^{n+1} = C_i^n + \frac{\Delta t^n}{\Theta_D} \frac{3 (F_{i+1}^{n+1} - F_i^{n+1})}{r_{i+1}^3 - r_i^3}. \quad (31)$$

where F_i^{n+1} represents the discrete flux between the cells $i - 1$ and i and, for $i = 1 \dots N - 1$, it is defined by:

$$F_i^{n+1} = \frac{2(r_i^{n+1})^2}{r_{i+1}^{n+1} - r_{i-1}^{n+1}} (C_i^m - C_{i-1}^m). \quad (32)$$

The discrete flux, F_N^{n+1} , at the external boundary of the influence region $r_N = S$, is given by the null flux condition on S :

$$F_N^{n+1} = 0 \quad (33)$$

and the Dirichlet boundary condition on the bubble-magma interface for $C(R, t)$, defines:

$$C_0^{n+1} = K_H \sqrt{P_i P^n}.$$

Concerning the discrete flux at the bubble-magma interface, F_0^{n+1} , we need to do some more work. As said, we want our numerical scheme to be preserving, i.e. to conserve the total water mass, since this fact is a direct derivation of the physical model. Let us then define, the discrete flux F_0^{n+1} by:

$$F_0^{n+1} = F_1^{n+1} - \frac{\Theta_D}{\Delta t^n} \frac{r_1^3 - r_0^3}{3} (C_0^{n+1} - C_0^n) \quad (34)$$

and the discrete total water mass \mathcal{M}^n by:

$$\mathcal{M}^n = M^n + \rho_m \sum_{i=0}^{N-1} C_i^n (r_{i+1}^3 - r_i^3). \quad (35)$$

Then we have:

Lemma 3.2 *The numerical scheme (23)-(34) conserves the discrete total water mass:*

$$\mathcal{M}^n = \mathcal{M}^0, \quad \forall n \in \mathbb{N}.$$

Proof: The total water mass at time t^{n+1} is equal to:

$$\mathcal{M}^{n+1} = M^{n+1} + \rho_m \sum_{i=0}^{N-1} C_i^{n+1} (r_{i+1}^3 - r_i^3).$$

Applying (24), splitting the sum for $i = 0$ and $i = 1 \dots N - 1$ and replacing (31) in the sum, we obtain:

$$\mathcal{M}^{n+1} = M^n + 3\rho_m \frac{\Delta t^n}{\Theta_D} F_0^{n+1} + \rho_m C_0^{n+1} (r_1^3 - r_0^3) +$$

$$+\rho_m \sum_{i=1}^{N-1} C_i^n (r_{i+1}^3 - r_i^3) + 3\rho_m \frac{\Delta t^n}{\Theta_D} \sum_{i=1}^{N-1} (F_{i+1}^{n+1} - F_i^{n+1}).$$

Hence, simplifying the last sum we get:

$$\begin{aligned} \mathcal{M}^{n+1} &= M^n + 3\rho_m \frac{\Delta t^n}{\Theta_D} F_0^{n+1} + \rho_m C_0^{n+1} (r_1^3 - r_0^3) + \\ &+\rho_m \sum_{i=1}^{N-1} C_i^n (r_{i+1}^3 - r_i^3) + 3\rho_m \frac{\Delta t^n}{\Theta_D} (F_N^{n+1} - F_1^{n+1}). \end{aligned}$$

Recalling that $F_N^n = 0$ for all n , and splitting, in the definition \mathcal{M}^n , the sum for $i = 0$ and $i = 1 \dots N - 1$, we must have that:

$$3\rho_m \frac{\Delta t^n}{\Theta_D} F_0^{n+1} + \rho_m C_0^{n+1} (r_1^3 - r_0^3) - 3\rho_m \frac{\Delta t^n}{\Theta_D} F_1^{n+1} = \rho_m C_0^{n+1} (r_1^3 - r_0^3),$$

which is verified since F_0^{n+1} is defined by (34). Hence, we have proved that for all n : $\mathcal{M}^{n+1} = \mathcal{M}^n$, so that the discrete total water mass is conserved. \square

Remark 3.1 *We note that the total water mass conservation is independent on the definition of the discrete flux inside the grid, F_i^n , for $i = 1 \dots N - 1$. We recall that definition (34), together with (29), are the crucial points enabling us to write a conservative numerical scheme. \square*

Before turning to the stability conditions for this scheme, we summarise here the main formula of the numerical approximation:

$$\begin{aligned} R^{n+1} &= \left(R^n - \Delta t^n \frac{\Sigma}{\Theta_V} \right) \left(1 - \Delta t^n \frac{(P^n - P_a^n)}{\Theta_V} \right)^{-1} \\ M^{n+1} &= M^n + 3\rho_m \frac{\Delta t^n}{\Theta_D} F_0^{n+1} \\ F_0^{n+1} &= F_1^{n+1} - \frac{\Theta_D}{\Delta t^n} \frac{r_1^3 - r_0^3}{3} (C_0^{n+1} - C_0^n) \\ F_i^{n+1} &= \frac{2 (r_i^{n+1})^2}{r_{i+1}^{n+1} - r_{i-1}^{n+1}} (C_i^n - C_{i-1}^n) \\ C_i^{n+1} &= C_i^n + \frac{\Delta t^n}{\Theta_D} \frac{3 (F_{i+1}^{n+1} - F_i^{n+1})}{r_{i+1}^3 - r_i^3} \\ r_i^{n+1} &= \left((R^{n+1})^3 - (R^n)^3 + (r_i^n)^3 \right)^{1/3} \end{aligned}$$

3.3 Stability conditions

In this section, we describe the stability conditions on the time step for our scheme. First, we compute the bounds for Δt^n for each numerical approximations, and then we take Δt^n the minimum of the three stability condition. Before dealing with equations (23) and (31), we note that we do not have a stability condition for the bubble mass approximation (24), but we ask that the discrete bubble pressure P^n remains larger than the ambient pressure P_a^n at each iteration n , which leads to:

$$\Delta t^n < \Theta_V \left| \frac{|(P_a^n - P^n)(R^3)^n - 3\rho_m(r_1^3 - r_0^3)C_0^n|}{|3\rho_m F_1^n|} \right| \quad (36)$$

Nevertheless, this condition is not sufficient to avoid oscillations in the solution, in some rare case, but permits in almost all cases to take reasonable time steps, i.e. $\Delta t^n \sim 10^{-9}$.

We look now for the stability conditions of (23) and (31). In particular we search a bound of the time step Δt^n such that each solution is positive.

Proposition 3.1 *Let $n \in \mathbb{N}$, if:*

$$\Delta t^n < \min \left(\frac{R^n \Theta_V}{\Sigma}, \frac{\Theta_V}{|P^n - P_a^n|} \right) \quad (37)$$

the solution to the numerical scheme (23) is positive, i.e. $R^n > 0$.

Proof: Let us assume that at the iteration n all the variables are positive, then at the iteration $n + 1$, using (23), Δt^n must be such that:

$$\left(R^n - \Delta t^n \frac{\Sigma}{\Theta_V} \right) \left(1 - \Delta t^n \frac{P^n - P_a^n}{\Theta_V} \right)^{-1} > 0.$$

We have two possibilities. The first one is when $P^n - P_a^n \leq 0$. Then we have:

$$1 - \Delta t^n \frac{P^n - P_a^n}{\Theta_V} > 0.$$

Hence,

$$R^n - \Delta t^n \frac{\Sigma}{\Theta_V} > 0$$

which implies,

$$\Delta t^n < \frac{\Theta_V R^n}{\Sigma}.$$

The second one is: $P^n - P_a^n > 0$. Then Δt^n must be the positive solution of a second order equation. The dominant coefficient:

$$\frac{\Sigma(P^n - P_a^n)}{\Theta_V^2}$$

is positive, hence R^{n+1} is positive, if Δt^n is external to the roots:

$$\frac{\Theta_V}{P^n - P_a^n}, \quad \frac{R^n \Theta_V}{\Sigma}.$$

Finally, we remark that the choice (37) verifies both conditions. \square

Proposition 3.2 *Let $n \in \mathbb{N}$, if:*

$$\Delta t^n < \frac{\Theta_D}{6} \min_i \left((r_{i+1}^3 - r_i^3) \left(\frac{r_{i+1}^{n+1} - r_{i-1}^{n+1}}{(r_i^{n+1})^2} \right) \right) \quad (38)$$

then the solution to the numerical scheme (31) is positive, i.e. $C_i^n > 0$ for all $i = 1 \dots N - 1$.

Proof: We first remark that the Dirichlet condition on the boundary $r = R$ implies that $C_0^n > 0$ for all $n \in \mathbb{N}$.

Assuming that at the n^{th} iteration C_i^n is positive for all $i = 0 \dots N - 1$, we want Δt^n to verify $C_i^{n+1} > 0$. Thus from (31), it must be, for $i = 1 \dots N - 1$:

$$C_i^n + \frac{3\Delta t^n}{\Theta_D(r_{i+1}^3 - r_i^3)} (F_{i+1}^{n+1} - F_i^{n+1}) > 0.$$

Recalling that F_i^{n+1} is given by (32), collecting the terms with respect to C_{i-1}^n , C_i^n and C_{i+1}^n and considering that C_i^n are positive for all i , we get a sufficient condition for the positivity of C_i^{n+1} in the form, for $i = 1 \dots N - 2$:

$$1 - \frac{6\Delta t^n}{\Theta_D(r_{i+1}^3 - r_i^3)} \left(\frac{(r_{i+1}^{n+1})^2}{r_{i+2}^{n+1} - r_i^{n+1}} + \frac{(r_i^{n+1})^2}{r_{i+1}^{n+1} - r_{i-1}^{n+1}} \right) > 0.$$

Since

$$\frac{r_{i+2}^{n+1} - r_i^{n+1}}{(r_{i+1}^{n+1})^2} > 0,$$

the time step Δt^n given by (38) verifies the above condition.

If now $i = N - 1$, recalling that $F_N^n = 0$ for all n , we obtain that Δt^n must satisfy:

$$\Delta t^n < \frac{\Theta_D}{6} (r_N^3 - r_{N-1}^3) \left(\frac{r_N^{n+1} - r_{N-2}^{n+1}}{(r_{N-1}^{n+1})^2} \right)$$

which conclude the proof. \square

4 Limit cases

As mentioned in section 2, the system of equation (21)-(22) we are considering has two relaxation times, Θ_V and Θ_D defined by (12), which may differ by several order of magnitude, depending on the values of, for instance, diffusivity or viscosity. In many experiments Θ_V and/or Θ_D are very small, on the order of 10^{-7} . The time steps Δt^n depending on these values, the computational time needed to reach a porosity close to 1 is very large. The study of the limit cases, such as when Θ_V and Θ_D tends to ∞ or to 0, is thus an attractive alternative to solving the full system because it leads to simplified models with smaller simulation times. In particular, we will classify the different limits in regimes of bubble growth by considering the ratio Θ_V/Θ_D . Following [10], we define a viscous regime when the ratio is very small, see 4.1, an equilibrium regime when the ratio is of order 1, see 4.2, and a diffusive regime when the ratio is large, see 4.3. At the end of each section, we will also summarise when necessary the numerical scheme corresponding to the simplified cases. As we are mainly interested in the behavior of the bubble physical dimensions (pressure P and radius R), we shall only describe how to compute these two quantities. In particular, we recall that, when comparing with experiments, we consider the porosity: $\alpha = R^3/S^3$. We list all the possible limits in table 2, which references each simplification to compute the bubble radius R and mass M (or pressure P). In table 2 we also give the orders of magnitude delimiting each regime.

Table 2: Limit cases

	∞			
		4.1.2 (42), (40)	4.1.1 (41), (40)	4.2.2 (49), (40)
Θ_D	10^3	4.1.3 (43), (44)	(14), (15)	4.3.1 (49), (50)
	10^{-3}	4.2.1 (43), (48)	4.3.3 (48), (14)	4.3.2 (49), (51)
		0	10^{-5}	10^1
			Θ_V	∞

4.1 Viscous regime : $\Theta_V/\Theta_D \ll 1$

We first look at the case when the viscous relaxation time is smaller than the diffusion one. There are three possibilities: Θ_V goes to zero and Θ_D is of order 1 or goes to infinity; and Θ_V is of order 1 and Θ_D goes to infinity.

4.1.1 $\Theta_V \sim 1$ and $\Theta_D \rightarrow \infty$

Since Θ_D is very large, equation (16) reads $r^2 d_t C(r, t) = 0$, which yields to:

$$\int_{R(t)}^{S(t)} r^2 C(r, t) dr = \int_{R(0)}^{S(0)} r^2 C_0 dr. \quad (39)$$

Concerning the bubble mass evolution, since $\Theta_D \gg 1$, equation (15) reads $\dot{M} = 0$, which is equivalent to:

$$M = M(0), \quad (40)$$

the water mass inside the bubble is constant. In fact, a large diffusive relaxation time may be physically given by a very small value for the diffusivity

in magma; hence there will not be diffusion of water from the magma into the bubble, and the bubble water mass will not change.

As $\Theta_V \sim 1$, no simplification is possible for the equation giving the evolution of the bubble radius (14). Still, recalling that $M(0) = M = PR^3$ and that the ambient pressure is given by (19), we can write a differential equation only depending on R :

$$\dot{R} = \frac{1}{\Theta_V} \left(\frac{M(0)}{R^2} - R(1-t) - \Sigma \right), \quad (41)$$

or equivalently on P :

$$\dot{P} = -\frac{3P}{\Theta_V} \left(P - (1-t) - \Sigma \left(\frac{P}{M(0)} \right)^{1/3} \right).$$

We note that we obtain the same result as in [10].

Numerically, since the mass $M = PR^3$ is constant, we simply solve equation (41) with an implicit scheme.

4.1.2 $\Theta_V \rightarrow 0$ and $\Theta_D \rightarrow \infty$

When Θ_D is large, the simplifications (39) and (40) are always true. In particular, water mass in the bubble is constant: $M = M(0)$.

Regarding equation (14), since Θ_V is very small, multiplying by Θ_V , recalling that $M(0) = PR^3$, and simplifying allows us to obtain a third order equation on R :

$$R^3(1-t) + \Sigma R^2 - P(0) = 0,$$

which admits an unique real solution given by:

$$R = \frac{c}{6a} + \frac{2b^2}{3ca} - \frac{b}{3a}, \quad (42)$$

where we have defined:

$$a = \frac{1-t}{P(0)}, \quad b = \frac{\Sigma}{P(0)}$$

and

$$c = \left(108a^2 - 8b^3 + 12\sqrt{3}\sqrt{27a^2 - 4b^3a} \right)^{1/3}.$$

In this case, since the mass M is constant, and the radius R is explicitly given by (42), no numerical scheme is needed.

4.1.3 $\Theta_V \rightarrow 0$ and $\Theta_D \sim 1$

If $\Theta_D \sim 1$, the simplifications of section 4.1.1 no longer hold. There is, for instance, no possible simplification for equations (15) and (16). Nevertheless, since $\Theta_V \ll 1$, we have:

$$P = 1 - t + \frac{\Sigma}{R} \quad (43)$$

which links the bubble pressure P to the radius R . On the other hand, considering that $M = PR^3$ and equation (15), we obtain the following differential equation for R :

$$\dot{R} = \left(\frac{3\rho_m}{\Theta_D} \left(r^2 \frac{\partial C}{\partial r} \right)_{r=R} + R^3 \right) (2\Sigma R + 3R^2(1-t))^{-1}, \quad (44)$$

where the water concentration is obtained solving the advection-diffusion equation (16).

Numerically, we respectively compute M^{n+1} and C_i^{m+1} using the general numerical schemes for equations (24) and (31), then we apply relation $M = PR^3$ to compute P and finally from (43) we obtain R .

4.2 Equilibrium regime: $\Theta_V/\Theta_D \sim 1$

In this section we deal with those regimes in which the relaxation times Θ_V and Θ_D are of the same order of magnitude. More precisely, when both Θ_V and Θ_D go to zero, or to ∞ , since otherwise no simplification is possible.

4.2.1 $\Theta_V \rightarrow 0$ and $\Theta_D \rightarrow 0$

This is an interesting situation because in this case computational time are very long and it corresponds to the equilibrium growth, which is a common situation in natural magmas (i.e. the bubble is always at its maximum possible radius).

Let us consider $\Theta_D \ll 1$, then multiplying the water concentration equation (16) by Θ_D and simplifying, we have:

$$\frac{1}{r^2} \frac{\partial}{\partial r} \left(r^2 \frac{\partial C}{\partial r} \right) = 0,$$

for which the solution, taking into account the boundary conditions (17) and (18), reads:

$$C(r, t) = C(R, t) = C_i \sqrt{P}, \quad \forall r \in [R(t), S(t)], \quad (45)$$

Thus, we see that when Θ_D tends to zero, equation (15) is not valid anymore to compute the water mass variation inside the bubble. Therefore, we consider the total mass conservation equation (13). Replacing C by (45) in (13), and recalling, (20), we obtain:

$$M = \rho_m S_0^3 (C_0 - C_i \sqrt{P}), \quad (46)$$

Now since $M = PR^3$, equation (46) is a second order equation in $X = \sqrt{P}$, with positive solution:

$$X = \frac{-Y + \sqrt{Y(Y + 4R^3 C_0 / C_i)}}{2R^3}$$

where we have posed:

$$Y = C_i \rho_m S_0^3. \quad (47)$$

This yields to the expression of P , as a function of R :

$$P = \left(\frac{-Y + \sqrt{Y(Y + 4R^3 C_0 / C_i)}}{2R^3} \right)^2, \quad (48)$$

with Y defined by (47).

On the other hand, since $\Theta_V \ll 1$, following the discussion of section 4.1.3, we have the simplification (43). Hence R and P are uniquely defined by (43) and (48).

Numerically, in order to avoid problems with the computation of the square root, we solve (43) and (46).

Remark 4.1 *We note that (48) may be expressed in terms of the porosity α . In fact, recalling that the porosity by $\alpha(t) = R^3/S^3$, we have:*

$$S_0^3 (R^3)^{-1} = \frac{1 - \alpha(t)}{\alpha(t)},$$

and thus:

$$P = \left(\frac{-Z + \sqrt{Z(Z + 4C_0 / C_i)}}{2} \right)^2,$$

with

$$Z = C_i \rho_m \frac{1 - \alpha}{\alpha}.$$

□

Remark 4.2 From the above simplification we get the following formula for the ambient pressure, P_a , as a function of R :

$$P_a = -\frac{\Sigma}{R} + \frac{W}{2} \left(C_i^2 W + 2C_0 - C_i \sqrt{W(C_i^2 W + 4C_0)} \right),$$

with:

$$W = \rho_m S_0^3 R^{-3}.$$

□

4.2.2 $\Theta_V \rightarrow \infty$ and $\Theta_D \rightarrow \infty$

In this situation, viscosity may be very large, yielding $\Theta_V \gg 1$, and diffusivity very small, implying $\Theta_D \gg 1$. Hence, following experimental evidence (see [7]), we can imagine that the physical system is "fixed" or "frozen".

On one hand, as discussed in section 4.1.1, the water mass in the bubble is constant, see equation (40). On the other hand, since $\Theta_V \gg 1$, from equation (14) we also obtain $\dot{R} = 0$, that is:

$$R(t) = R(0) = 1. \quad (49)$$

Since both the mass M and the radius R are constant, the pressure P is explicitly determined by $M = PR^3$, and no numerical scheme is needed.

4.3 Diffusive regime : $\Theta_V/\Theta_D \gg 1$

In this last section, we treat regimes which have the viscous Θ_V relaxation time larger than the diffusion one Θ_D . We have to differentiate three cases: when Θ_D is small and Θ_V is of order one or goes to infinity, and when Θ_D is of order one and Θ_V goes to infinity.

4.3.1 $\Theta_V \rightarrow \infty$ and $\Theta_D \sim 1$

As shown before, when $\Theta_V \rightarrow \infty$, we obtain equation (49). Hence, the bubble radius is constant in time, and recalling that $M = PR^3$, we have $\dot{M} = \dot{P}$, hence from (15) we get the following differential equation on P :

$$\dot{P} = \frac{3\rho_m}{\Theta_D} \left(r^2 \frac{\partial C}{\partial r} \right)_{r=R}, \quad (50)$$

with C solution of (16).

Numerically, the radius R is constant, and the pressure P is computed using the numerical scheme of section 3.

4.3.2 $\Theta_V \rightarrow \infty$ and $\Theta_D \rightarrow 0$

Considering the discussion of sections 4.2.2 and 4.2.1, we have that the simplifications (49) and (48) hold. From (49), the bubble radius is constant, $R = 1$, then because of (48), the bubble pressure is also constant in time and is given by:

$$P = \left(\frac{-Y + \sqrt{Y(Y + 4C_0/C_i)}}{2} \right), \quad (51)$$

with Y given by (47).

Once again, the radius R is constant while the pressure P is explicitly given by the formula (51).

4.3.3 $\Theta_V \sim 1$ and $\Theta_D \rightarrow 0$

Since $\Theta_V \sim 1$, there is no possible simplification for equation (14). On the other hand, from section 4.2.1, the bubble pressure is computed by (48).

In this case, the radius R must be computed using the numerical scheme of section 3, while the pressure P is explicitly given by (48).

5 Numerical results

We performed some numerical tests based on the schemes described in sections 3 and 4. In this section we compare first the numerical results obtained using the general scheme of section 3 to those obtained with the numerical approximation of the simplified schemes of section 4. This is followed by a comparison between the behavior of our numerical results and experimental data described in [2].

Let us first discuss the dependence of our results on the number of discretization points N with respect to the radial variable r . As announced previously, various numerical tests show that a small number of points is sufficient in order to well capture the behavior of the discrete flux F_0^n on the bubble border. The relative errors of the curves for the bubble radius R , bubble pressure P , and porosity α with respect to the reference ones with $N = 2500$, are of order 10^{-3} for $N = 50$ and of order 10^{-4} for $N = 250$, respectively. We therefore choose $N = 50$ in all the following computations.

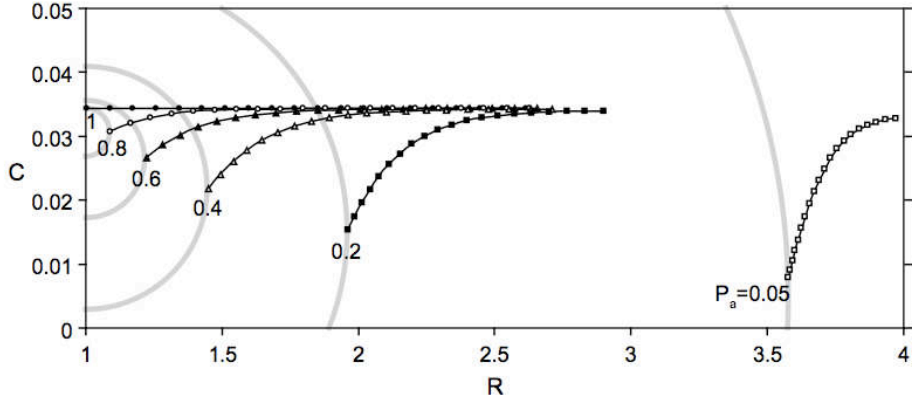


Figure 1: Bubble growth and gas concentration function in the influence region.

In figure 1 we show the evolution of the concentration function $C(t, r)$ computed solving the general scheme with $\Theta_V = 0.000236$ and $\Theta_D = 5.28929$. Bubble size evolution is sketched as grey circles of increasing radius R . We clearly see the mesh refinement near the bubble wall (the grey circle portion) when the concentration function becomes stiffer.

5.1 Numerical convergence

We show now through a few selected examples the numerical convergence of the global numerical scheme defined in section 3 towards the simplified limit cases discussed in section 4. Convergence is determined by fixing either the value of Θ_V or Θ_D and varying the other one. This crossed method yields the Θ_V and Θ_D orders of magnitude for which the system changes regime. We can see in table 2 that for $\Theta_V < 10^{-5}$ and $\Theta_D < 10^{-3}$ we have the so called equilibrium regime, whereas for $\Theta_V > 10^2$ and for each Θ_D the bubble radius must be constant. These results suggest that the simplified limit cases are sufficient for a good description of the physical system. Their use significantly reduces computation time.

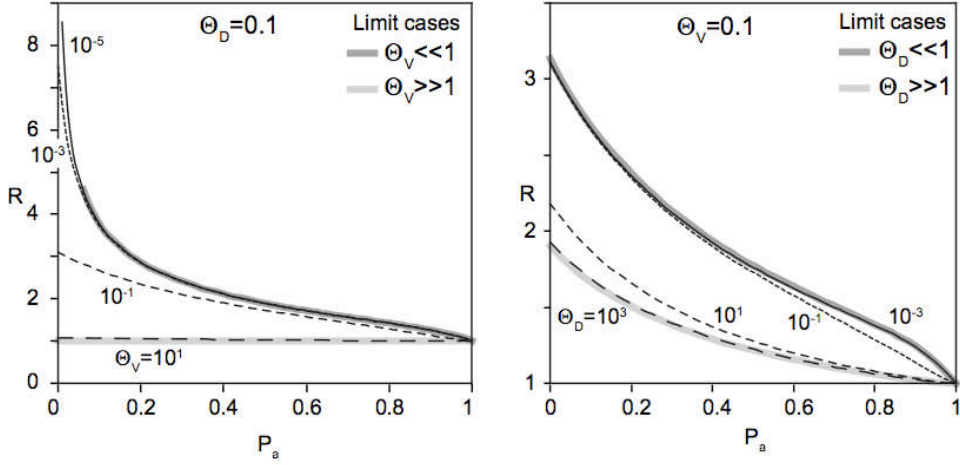


Figure 2: Bubble radius evolution and convergence. Left: convergence towards the limit cases 4.1.3 and 4.3.1. Right: convergence towards the limit case 4.1.1 and 4.3.3.

In figure 2 we show the convergence for the bubble radius towards selected limit cases. On the left, we plot the bubble radius evolution with respect to the ambient pressure P_a (we recall that ambient pressure linearly decreases in time as $1-t$), fixing $\Theta_D = 0.1$ and varying Θ_V from 10^{-5} to 10^1 , together with the radius computed as explained in 4.1.3 or just defined as the constant 1, as justified in 4.3.1. On the right, we plot the bubble radius evolution with respect to time, fixing $\Theta_V = 0.1$ and varying Θ_D from 10^{-3} to 10^3 , together with the radius obtained as explained in 4.1.1 and 4.3.3. In both cases we can observe the transition of the general unsimplified regime (the middle case in table 2) from one simple growth regime to the next.

5.2 Experiments vs. numeric

Controlled decompression experiments on high temperature magmas are able to produce gas bubbles. By varying the end pressure, data on bubble size and porosity have been retrieved for different initial condition such as magma viscosity, temperature, decompression rate, etc. In this work we illustrate how comparisons between such experimental data and model outputs can be carried out. Let us first present here the experimental framework used by [2]. Samples of viscous magma are saturated in water and maintained under pressure for about 5 days for the water to homogeneously dissolved into the magma. Then an instantaneous decompression gives rise to bubble nucleation. After waiting for a few minutes that these initial, small bubble

reach their equilibrium sizes, a linear decompression is applied until a final pressure where samples are quenched by a sudden cooling to ambient temperature. The cold samples are then sliced and analysed to obtain bubble sizes and porosity. One experiment quenched just after the sudden decompression that nucleates the bubbles gives the initial conditions for our model.

The physical values used and measured during the experiments are the following: the initial radius $R_i = 17.5 \cdot 10^{-6}$, the diffusion coefficient $D_i = 5.79 \cdot 10^{-12}$, the initial concentration $C_0 = 3.44 \cdot 10^{-2}$, the initial pressure $P_i = 10^8$, the surface tension $\sigma = 0.1$, the viscosity $\eta_i = 5.9 \cdot 10^{-4}$, the magma density $\rho_m = 2400$, the gas porosity density ρ_i being calculated by the perfect gas law (3), the temperature $T = 825$, and the decompression rate $\Delta P = 10^{-5}$. We tested two different experimental series. In the first series, bubbles growth was only due to gas expansion and water diffusion from the magma. In the second series, bubbles growth was also due to coalescence processes. The porosity evolution of both series is comparable but the evolution of bubble size differ.

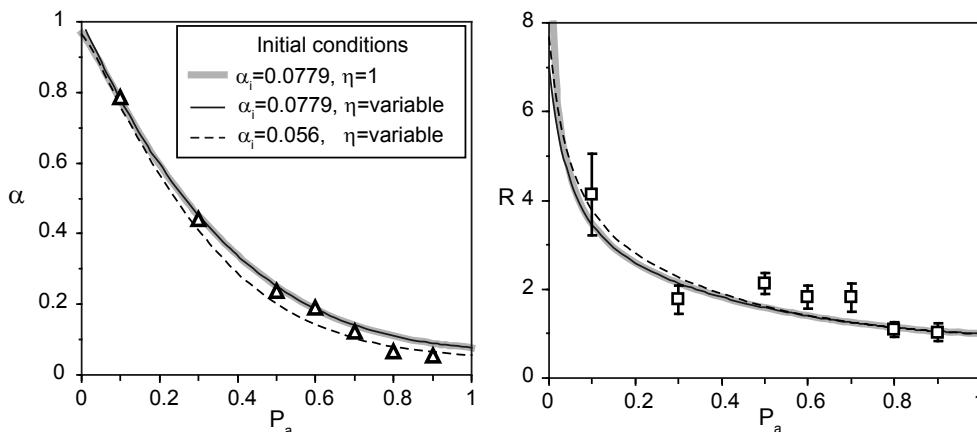


Figure 3: Porosity α (on the left) and radius R (on the right) with respect to ambient pressure P_a : effect of a variable viscosity η_{eff} .

In figure 3 we show the evolution of the porosity α and of the radius R with respect to the ambient pressure P_a . On the left graph are represented three numerical results for different viscosity calculation and initial porosities along with the experimental results obtained in [2] (triangles). The run represented by the grey line had a constant viscosity η , whereas the black line and the dashed line had variable viscosity η_{eff} computed applying the formula given in [8, 10]. We remark that considering a variable viscosity η_{eff} instead of a

constant one has an impact on the numerical result only when the ambient pressure becomes very small because the grey and the black curves diverge only when $P_a < 0.1$. The dashed line is a numerical result computed starting from the porosity measured on the experiment quenched just after the sudden decompression. The two other runs use the equilibrium state (see Remark 4.1 below), which predicts a porosity of 0.0779 instead of 0.056. We note that the experimental points fit better the dashed line at high P_a and are closer to the two other curves at low P_a . This lead us to conclude that during the first phase of the experiments the time waited between nucleation and the beginning of the decompression was not enough to reach the equilibrium. The right graph shows the numerical radii R as a function of the ambient pressure P_a for the same three numerical runs (on the left). Experimental results are now represented with square points centred on the median value of the experimental radii together with a standard deviation representing the spread of measured bubble radii. We note that the three runs are very similar, regardless of initial conditions, and that the fit between experiments and numerical results is worst for radius than porosity. The larger misalignment of experimental radii compared to that of porosity is explained by the fact that each experimental point in figure 3 is a full decompression run starting from $P_a = 1$. As a result, bubble nucleation dynamics occurring during the initial decompression step is only approximately similar from one experiment to the next.

Remark 5.1 *As discussed in section 4.2.1, we have an equilibrium state when Θ_V and Θ_D are small. The most commonly used formula to calculate porosity is (e.g., [9]):*

$$\alpha_{eq} = \frac{\beta}{1 + \beta} \quad (52)$$

where:

$$\beta = K_H(\sqrt{P_0} - \sqrt{P_a})$$

with P_0 is the ambient pressure when all bubbles have radius $R = 0$.

We note that, from the simplification of section 4.2.1, we can derive a formula for the porosity α , similar to the previous one (52):

$$\alpha = \frac{K}{P + K},$$

where:

$$K = \rho_m \left(C_0 - C_i \sqrt{P} \right)$$

and now the pressure P takes into account also the surface tension term: $P = P_a + \Sigma/R$.

Finally, the porosity at equilibrium computed with our formula exactly reproduces the one given by experiments, see (52). \square

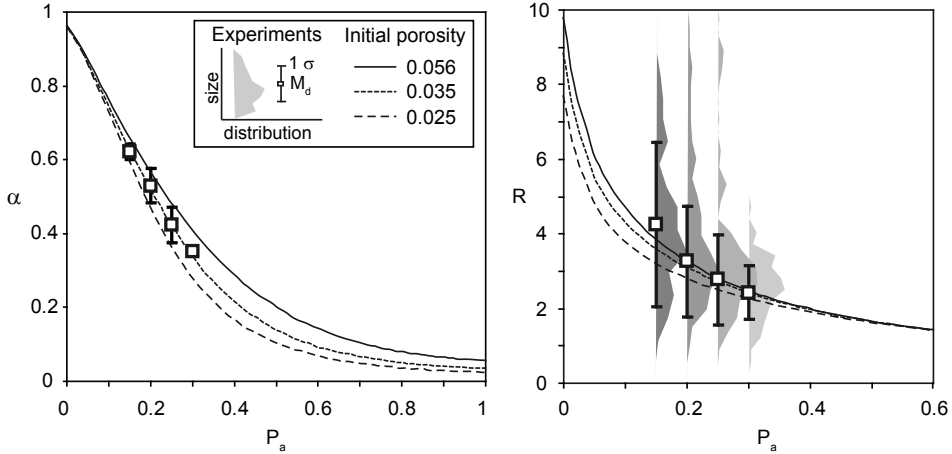


Figure 4: Bubble radius R with respect to ambient pressure P_a : mono-disperse vs. poly-disperse.

In figure 4 we compare the experimental results obtained in [2] when bubble coalescence occurs with our numerical results with variable viscosity for three different initial porosities. The left graph, which displays the evolution of porosity with ambient pressure, indicates that this experimental series is best reproduced numerically by starting from a initial porosity of 0.035. This is lower than the best fit value of the other series. A tentative explanation of this situation is a even shorter pause between bubble nucleation and the start of the decompression. We plotted on the right graph, which shows the evolution of R with ambient pressure, distribution histograms of measured bubble radii. The three computed bubble radius R all fit the experimental measurements within a standard deviation, but, considering the large spread of bubble sizes, it is not possible to choose which numerical results has the better fit. As discussed in [2], this layout is due to the poly-disperse nature of bubble growth in the experiments, which was caused by bubble coalescence. Hence, in order to produce more accurate results that resolve the spread in bubble sizes, one should consider poly-disperse modelling of the bubbles population.

Further comparisons with other experimental results is under investigation and will be exposed in a future work. We simply underline herein that

our numerical code has a satisfactory behavior when confronted to various experimental works, and that it is sufficiently accurate to point experimental shortcomings as long as poly-disperse processes do not dominate bubble growth.

6 Conclusions

In the present paper, we have proposed and applied a numerical scheme for the approximation and simulation of the solution of a non-linear system of differential equations coupled with an advection diffusion equation, popularised in the volcanology literature by [12] and [10]. Our goals were twofold: give a conservative discretization of the system and study the asymptotic limits when the two relaxation times Θ_V and Θ_D went to 0 or ∞ .

In the recent years (see for example [5] and the reference therein), the numerical approach to solve the model governed by equations (21)-(22) is based on the one proposed in [14]: the transport term in the advection-diffusion equation is simplified by the means of a change of variable at the continuum level, leading to a kind of heat equation (the diffusion term is not standard). Nevertheless, with the method proposed in [12], a large number N of discretisation points in the radial direction is greatly reduced by the means of a variable mesh size. This size is controlled by an empirically defined parameter that ensures the conservation of water mass and that precisely captures the behavior of the flux on the bubble border. With our approach, a small number of points, $N = 50$, also guarantees precise results, but the mesh size is automatically defined. In fact, the discrete flux on the bubble border is defined in such a way that the numerical scheme preserves water mass (see Lemma 3.2). There is thus no need to adjust an empirical parameter to ensure scheme accuracy.

Concerning the asymptotic behavior of the coupled system of equations, we have analytically deduced the different simplified models in the three regimes: viscous, when $\Theta_V/\Theta_D \ll 1$, diffusive, when $\Theta_V/\Theta_D \gg 1$, and in the equilibrium one, when $\Theta_V/\Theta_D \sim 1$. In particular, when both Θ_V and Θ_D go to 0, we retrieve the equilibrium state of the problem. We have numerically shown the convergence of the scheme towards the solutions of the three regimes when varying the relaxation times. We also determined numerically the boundaries between the various regimes.

We finally compare our numerical results with data obtained from decompression experiments of natural magmas. This validation of the code gives also a feedback on the quality of experimental results. In particular, we show that, unlike originally assumed by the authors, decompressions in [2] started

while bubbles were still growing, i.e. equilibrium was not reached. Finally, it appears that the simplified mono-disperse framework is not accurate enough (see figure 4) to capture spreading bubble size distributions such as those produced by bubble coalescence. We thus infer that an extension of the physical model to include a poly-disperse description for the bubbles population is a worthy pursuit.

Acknowledgments

This work was partially founded by the ERC-starting grant DEMONS (n. 202844) under the European FP7.

References

- [1] A. Arefmanesh, and S.G. Advani, Diffusion-induced growth of a gas bubble in a viscoelastic fluid. *Rheol. Acta* **30** (1991) 274-283.
- [2] A. Burgisser, J.E. Gardner, Experimental constraints on degassing and permeability in volcanic conduit flow. *Bull. Volcanol.* **67** (2005) 42-56.
- [3] T. Beechem, K. Lafdi, and A. Elgafy, Bubble growth mechanism in carbon foams. *Carbon* **43** (2005) 1055-1064.
- [4] J.D. Blower, H.M. Mader, and S.D.R. Wilson, Coupling of viscous and diffusive controls on bubble growth during explosive volcanic eruptions. *Earth and Planetary Science Letters* **193** (2001) 47-56.
- [5] B. Chouet, P. Dawson, and M. Nakano, Dynamics of diffusive bubble growth and pressure recovery in a bubbly rhyolitic melt embedded in an elastic solid. *J. Geophys. Res.* **111** B07310 (2006) .
- [6] J.E. Gardner, The impact of pre-existing gas on the ascent of explosively erupted magma. *Bull. Volcanol.* **71** (2009) 835-844.
- [7] J.E. Gardner, M. Hilton, and M.R. Carroll, Bubble growth in highly viscous silicate melts during continuous decompression from high pressure. *Geochimica et Cosmochimica Acta* **64** (2000) 1473-1483.
- [8] K-U. Hess and D.B. Dingwell, Viscosities of hydrous leucogranitic melts: a non-Arrhenian model. *American Mineralogist* **81** (1996) 1297-1300.

- [9] C. Jaupart, and C. Allegre, Gas content, eruption rate and instabilities of eruption regime in silicic volcanoes. *Earth and Planetary Science Letters* **102** (1991) 413-429.
- [10] N.G. Lensky, O. Navon, and V. Lyakhovsky, Bubble growth during decompression of magma : experimental and theoretical investigation. *J. Volc. Geoth. Res.* **129** (2004) 7-22.
- [11] A.A. Proussevitch, and D.L. Sahagian, Dynamics and energetics of bubble growth in magmas: Analytical formulation and numerical modeling. *J. Geophys. Res.* **103** (1998) 18223-18251.
- [12] A.A. Proussevitch, D.L. Sahagian, and A.T. Anderson, Dynamics of diffusive bubble growth in magma: isothermal case. *J. Geophys. Res.* **98** (1993) 22283-22307.
- [13] G. Rosebrock, A. Elgafy, T. Beechem, and K. Lafdi, Study of the growth and motion of graphitic foam bubbles. *Carbon* **43** (2005) 3075-3087.
- [14] L.E. Scriven, On the dynamics of phase growth. *Chemical Engineering Science* **10** (1959) 1-13.
- [15] A. Toramaru, Numerical study of nucleation and growth of bubbles in viscous magmas. *J. Geophys. Res.* **100** (1995) 1913-1931.
- [16] J.S. Vrentas, and C.M. Vrentas, Slow bubble growth and dissolution in a viscoelastic fluid. *J. Appl. Polymer Sc.* **67** (1998) 2093-2103.
- [17] S.W.J. Welch, Direct simulation of vapor bubble growth. *International Journal of Heat and Mass Transfer* **41** (1998) 1655-1666.